Stabilization of biskyrmions by chiral interaction in centrosymmetric magnets

Deepak S. Kathyat and Pinaki Sengupta
School of Physical and Mathematical Sciences, Nanyang Technological University, Singapore

(Received 3 June 2024; accepted 19 September 2024; published 4 October 2024)

We report a microscopic mechanism for stabilization of biskyrmions in two dimensions by investigating a minimal model of classical spins on a triangular lattice with nearest-neighbor ferromagnetic Heisenberg exchange and static chiral interaction on each triangular plaquette. Our results establish that the chiral magnetic interaction results in biskyrmion states above a critical value, and its strength affects the size of the biskyrmions forming. We further explore the effects of thermal fluctuations on the biskyrmion states.

DOI: 10.1103/PhysRevB.110.144409

I. INTRODUCTION

Topologically protected magnetic textures like skyrmions and antiskyrmions can enable spintronic applications for building information storage and processing devices in the future [1–6]. Till date such textures were observed in a wide range of materials in various experimental studies [7–23]. The absence of inversion symmetry breaking in centrosymmetric materials forbids Dzyaloshinskii-Moriya interaction (DMI). In these materials, the skyrmion crystals get stabilized by competing exchange interactions coming from geometrical frustration of the short-range two-spin interactions, hence termed as chiral geometric frustration [24–27] or magnetic anisotropies [28]. In noncentrosymmetric crystals, the formation of these textures is understood theoretically via the interplay between Heisenberg exchange and DMI found in materials lacking inversion symmetry [29–35]. In metallic magnets with noncentrosymmetric geometry, the relevant microscopic models feature spin-orbit coupling of itinerant electrons [36–41]. Recent studies have elucidated the connection between topological magnetic textures and the underlying electronic band structure in metallic magnets [42,43]. Such magnetic textures can be controlled using ultralow currents in metals. In contrast, complex magnetic textures affect the electronic properties by inducing emergent magnetic fields acting on conduction electrons by imparting a Berry phase and lead to magnetoelectric phenomena such as the colossal magnetoresistance and the topological Hall effect [41]. At very low current densities, these magnetic textures lead to large spin-transfer torques, which have substantial implications for spintronic applications. Antiferromagnetic skyrmions, which are essentially a configurational linear combination of an antiferromagnet and a skyrmion, have also been studied [43–46]. The advantage of antiferromagnetic skyrmions over Skyrmions is that they do not experience transverse deflection upon application of current, known as Skyrmion Hall effect.

Topological magnetic textures are described by an integer, known as topological charge or topological number, n_{sk} which is defined as the integral of the solid angles spanned by the three neighboring spins and is given by [47]

$$n_{sk} = \frac{1}{4\pi} \int d^2r (\partial_x \mathbf{m} \times \partial_y \mathbf{m}) \cdot \mathbf{m}, \tag{1}$$

where $\mathbf{m}$ is a unit vector pointing in the direction of the magnetization. The topological charge describes how many times magnetic moments wrap around a unit sphere upon application of stereographic projection. As a consequence, skyrmions possess topological protection since erasing a skyrmion requires globally modifying the system—local changes in spin configurations are not sufficient. Skyrmions and antiskyrmions have opposite topological charges of ± 1. Skyrmions with higher n_{sk} can bring about richer physics. For example, a large topological Hall effect can be observed because of the larger spin noncoplanarity, which can induce larger emergent electromagnetic fields for the conduction electrons [48]. They may also allow multiple digital control of the topological numbers.

Biskyrmions, the magnetic textures of $n_{sk} = \pm 2$ are composed of two bound skyrmions of oppositely swirling spins (magnetic helicities) and are rarely found. The first real space observation of biskyrmions was shown using Lorentz transmission electron microscopy (LTEM) in 2014 in a thin plate of bilayer manganite $La_{2-2x}Sr_{1+2x}Mn_2O_7$ with uniaxial magnetic anisotropy [49]. It was also demonstrated that biskyrmions can be electrically driven with a much lower current density as compared to the conventional ferromagnetic domain walls. Later, these textures were observed in other centrosymmetric magnets such as MnNiGa, Nd_2Co_{17} [50,51]. However, there is an ongoing debate on the observations of biskyrmion crystals by LTEM imaging. In two recent publications, the authors showed that the tilting effect can also be responsible for the unique Lorentz contrast. Tubes of topologically trivial bubbles appear as skyrmion pairs with reversed in-plane magnetizations when viewed under an angle [52,53]. Several theories have been put forward to explain the stabilization mechanism of biskyrmions [48,54–58]. Gobel *et al.* postulated on the stabilization of biskyrnmions by dipole-dipole interacion. This is present in all magnetic materials, but gets overshadowed by DMI in noncentrosymmetric materials. In centrosymmetric materials, a short range dipole-dipole interaction leads to the attraction of two skyrmions resulting in the formation of biskyrmions which is energetically preferable over two individual skyrmions [54]. Biskyrmions arranged in a triangular lattice are found to exist as a result of the competing nearest-neighbor exchange

interaction, perpendicular magnetic anisotropy, dipole-dipole interaction, and the applied external magnetic field [55,56]. In addition to insulating magnets, biskyrmions are also found to be stable in itinerant magnets at zero magnetic fields. The Ruderman-Kittel-Kasuya-Yosida (RKKY) interaction between the localized magnetic moments mediated by conduction electrons plays a crucial role in stabilizing biskyrmions as shown using modified kernel polynomial method with Langevin dynamics (KPM-LD) simulations [48,57]. The formation of biskyrmions mediated by an intrinsic emergent monopole-antimonopole pair has been demonstrated using micromagnetic simulations [58].

In this work, we study the classical Heisenberg model with an additional time-reversal symmetry breaking chiral interaction [59] on a centrosymmetric triangular lattice and show the emergence of biskyrmions. Our focus is on the magnetic ground states and thermally stabilized topological magnetic textures. The appearance of biskyrmions is explicitly demonstrated using the state-of-the-art classical Monte Carlo simulations. We show that the competing nearest-neighbor exchange interaction and scalar chiral magnetic interaction give rise to the emergence of biskyrmions.

II. MODEL AND METHOD

We start with an effective spin model on a triangular lattice [60,61],

$$H = J_H \sum_{\langle i,j \rangle} \mathbf{S}_i \cdot \mathbf{S}_j + J_C \sum_{i,j,k \in \triangle} \mathbf{S}_i \cdot (\mathbf{S}_j \times \mathbf{S}_k). \tag{2}$$

The first term in the Hamiltonian Eq. (2) is the Heisenberg exchange interaction with coupling, J_H, between spins at nearest-neighbor sites $\langle ij \rangle$. The second term is chiral magnetic interaction with coupling strength, J_C. i, j, k are sites in a counterclockwise direction around each elementary triangle. This term is often studied to understand the chiral topological spin liquid phase in systems with quantum spins [59,61–63]. In this study, we extend such an interaction to classical spins. In materials such as $La_{2-2x}Sr_{1+2x}Mn_2O_7$, MnNiGa, Nd_2Co_{17} where biskyrmions were observed [49–51], the localized magnetic moments arose from partiallly filled d or f orbitals. This results in large moments and the localized spins can be approximated as classical vectors.

We compute the component-resolved spin structure factor (SSF) to characterize the ordered magnetic phases. The components of SSF are given by

$$S_f^{\mu}(\mathbf{q}) = \frac{1}{N^2} \left\langle \sum_{ij} S_i^{\mu} S_j^{\mu} \, e^{-i\mathbf{q}\cdot(\mathbf{r}_i - \mathbf{r}_j)} \right\rangle, \tag{3}$$

with $\mu = x, y, z$. The total SSF is $S_f(\mathbf{q}) = S_f^x(\mathbf{q}) + S_f^y(\mathbf{q}) + S_f^z(\mathbf{q})$.

We also calculate the discretized version of topological charge called as skyrmion density, $\mathscr{T}$, given by [45]

$$\mathscr{T} = \frac{1}{4\pi} \left\langle \sum_i A_i^{(12)} \mathrm{sgn}\left[\mathscr{L}_i^{(12)}\right] + A_i^{(45)} \mathrm{sgn}\left[\mathscr{L}_i^{(45)}\right] \right\rangle, \tag{4}$$

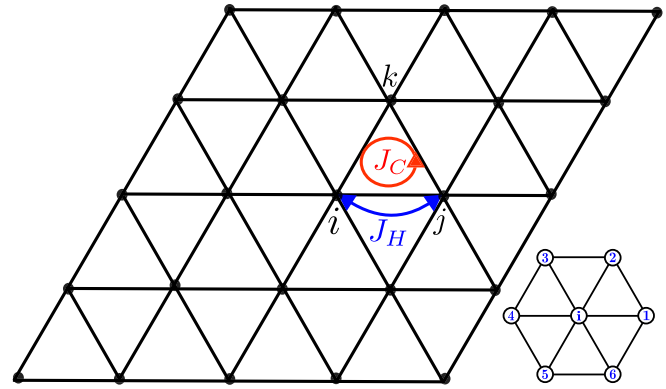

FIG. 1. Schematic diagram showing various terms in the Hamiltonian. In a triangular lattice, J_H is nearest-neighbor ferromagnetic exchange interaction between sites i and j. J_C is the chiral magnetic interaction for each elementary triangle of the lattice with sites i, j, and k in an anticlockwise direction. The right bottom panel shows the sites involved in the calculation of local skyrmion density $\mathscr{T}_i$ at site i.

which is total of the local skyrmion densities, $\mathscr{T}_i$ at each lattice site

$$\mathscr{L} = \frac{1}{8\pi} \left\langle \sum_i \mathscr{L}_i^{(12)} + \mathscr{L}_i^{(45)} \right\rangle, \tag{5}$$

where, $A_i^{(ab)} = ||(\mathbf{S}_{i_a} - \mathbf{S}_i) \times (\mathbf{S}_{i_b} - \mathbf{S}_i)||/2$ is the local area of the surface spanned by three spins on every elementary triangular plaquette $\mathbf{r}_i, \mathbf{r}_a, \mathbf{r}_b$. Here $\mathscr{L}_i^{(ab)} = \mathbf{S}_i.(\mathbf{S}_{i_a} \times \mathbf{S}_{i_b})$ is the so-called local chirality and $\mathbf{r}_i, \mathbf{r}_1 - \mathbf{r}_5$ (see right bottom panel Fig. 1) are the sites involved in the calculation of $\mathscr{T}$.

III. RESULTS

The first term in the Hamiltonian Eq. (2) is the Heisenberg model, which has a ferromagnetic ground state for $J_H = -1.0$. We investigate the effect of chiral magnetic interaction on the ferromagnetic exchange Heisenberg model. We use classical Monte Carlo simulations with the standard METROPOLIS algorithm. The simulations are carried out on lattice sizes varying from $N = 40^2$ to $N = 100^2$, and $\sim 5 \times 10^4$ Monte Carlo steps are used for equilibration and averaging at each temperature point. Spin configurations in the magnetic states obtained at low temperature ($T = 0.001$, where T is expressed in units of $|J_H|$) are shown for lattice size $N = 24^2$ for $J_C = 1.0$ in [see Fig. 2(a)] and $J_C = -1.0$ in [see Fig. 2(d)]. We can clearly see the stabilization of Bloch biskyrmions in both cases. The central spins of biskyrmions in the [Fig. 2(a)] are pointing down while the biskyrmions in the [Fig. 2(d)] have central spins pointing up. The spin structure factor for both the magnetic configurations [see Figs. 2(b) and 2(e)] shows the hexagonal peaks in the first Brillouin zone. The quantity that differentiates these two types of biskyrmions is their skyrmion density $\mathscr{T}$. Local skyrmion density maps on the lattice are shown in [Figs. 2(c) and 2(f)] corresponding to the magnetic textures in [Figs. 2(a) and 2(d)], respectively. An ideal biskyrmion of type [Fig. 2(a) has $n_{sk} = -2$ as the central spin is pointing

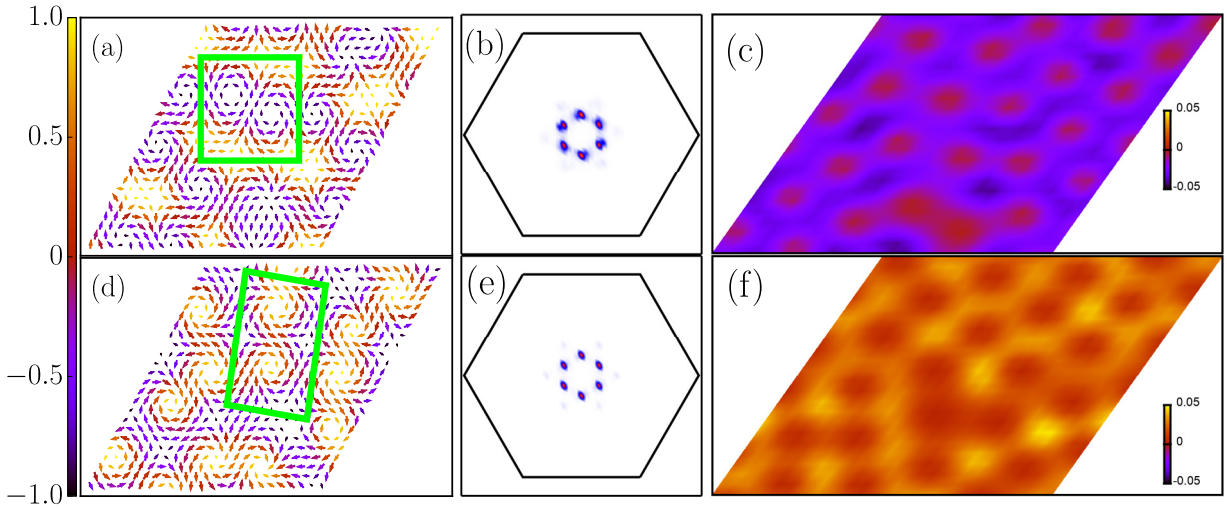

FIG. 2. Ground-state spin configurations at low temperature ($T = 0.001$) for (a) $J_C = 1.0$ and (d) $J_C = -1.0$ on triangular lattice of size $N = 24^2$. The green box highlights the biskyrmions in both cases. (b) and (e) are the spin structure factor plots corresponding to magnetic states (a) and (d), respectively. (c) and (f) shows the corresponding local skyrmion density $\mathscr{T}_i$ maps on the lattice.

down. The corresponding skyrmion densities are negative on the local skyrmion density map. Similarly, in [Fig. 2(f)], local skyrmion densities are positive for the biskyrmions with $n_{sk} = +2$.

Results from large scale Monte Carlo simulations of the Hamiltonian (2) are presented in Figs. 3 and 4. Figure 3(a) shows the variation of energy per site and Skyrmion density, $\mathscr{T}$, as a function of temperature as we cool down the system from a high temperature to $T = 0.001$. Figure 4 shows the static spin structure factor in the first Brillouin zone for three representative values of T. At high temperatures ($T \gtrsim 2.0$), there exists no long-range magnetic order, as seen from the SSF at $T = 1.25$ [Fig. 4(a)] that is marked by the absence of any clear structure. However, the Skyrmion densities are finite, reflecting the presence of short-range correlation driven by the chiral interaction. As the temperature is decreased, the Skyrmion density exhibits a broad local minimum around $T \approx 1.1$ and the energy curve shows an inflexion point. In this temperature range ($0.55 \lesssim T \lesssim 2.0$), the magnetic states consist of chiral filaments that consitute fragments of the biskyrmions. Alternatively, this state can be viewed as thermal fluctuations of biskyrmion states as shown in Fig. 3(b).

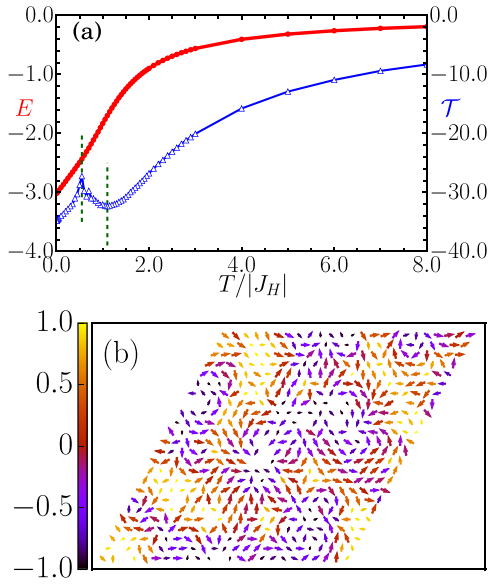

FIG. 3. (a) Variation of energy per site (red circles) and skyrmion density, $\mathscr{T}$ (blue triangles) with decreasing temperature. Vertical dashed lines mark a crossover behavior at temperature at $T = 1.1$ and transition at $T = 0.55$. (b) Magnetic states stabilize in between these two temperatures.

The SSF at $T = 0.6$ displays a diffused circular ring pattern without any prominent peaks, suggestive of a filament-like magnetic state. With further cooling, there is a transition to the biskyrmion ground state at $T = 0.55$, marked by a cusp in the Skyrmion number graph. Below this temperature, biskyrmions are well formed and form a periodic pattern. The SSF at $T = 0.01$ confirms that biskyrmions are well ordered and closely packed have peaks with an hexagonal symmetry at this temperature.

Next, we explore how the strength of chiral magnetic interaction affects the stabilization of biskyrmions. In the [Fig. 5(a)], the variation of skyrmion density, $\mathscr{T}$ with $J_C/|J_H|$ is shown. Varying J_C with $J_H = -1.0$ is taken for this calculation. We can see that below a critical value of J_C that is 0.8, the

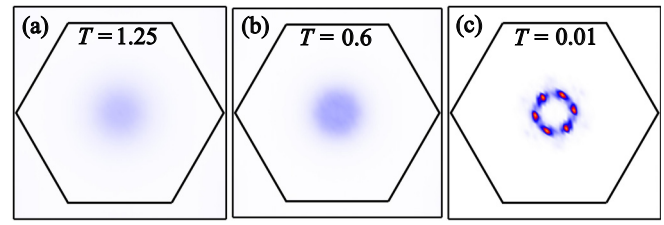

FIG. 4. Spin structure factor plots in the first Brillouin zone at different temperatures (a) at $T = 1.25$, (b) at $T = 0.6$, and (c) at $T = 0.01$.

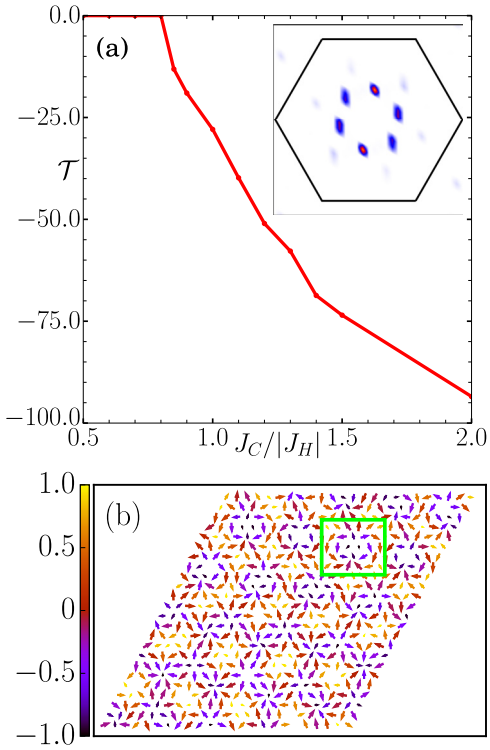

FIG. 5. (a) Skyrmion density, $\mathscr{T}$ versus $J_C/|J_H|$ plot with $J_H = -1.0$ fixed. (b) Magnetic ground state at $J_C = 1.5$. Inset in (a) shows the spin structure factor plot corresponding to the spin configuration in (b).

ground state is ferromagnetic with $\mathscr{T} = 0.0$. Above this critical value, we get the biskyrmions, and as the $J_C/|J_H|$ increases $\mathscr{T}$ also increases. This happens because of the increase in the number of biskyrmions as shown in [Fig. 5(b)] for the case of $J_C/|J_H| = 1.5$. We can also see that with increasing strength of $J_C/|J_H|$, the size of the biskyrmions decreases. This decrease in the size of bisyrmions is also reflected in the corresponding spin structure factor plot shown in the inset of [Fig. 5(a)]. The hexagonal peaks in the spin structure factor occur at large **Q** as compared to the peaks in [see Figs. 2(b) and 2(e)].

IV. CONCLUSION

We presented a mechanism for the stabilization of biskyrmions driven by chiral spin interaction by investigating a minimal classical spin model. Using large-scale Monte Carlo simulations, we demonstrated the emergence of bisyrmions on a triangular lattice with competing nearest-neighbor ferromagnetic Heisenberg exchange and a chiral spin interaction defined on the triangular plaquettes. The model can be generalized to other two-dimensional lattices. We identified the biskyrmions by their real-space spin configuration maps and the corresponding hexagonal peaks in the static spin structure factor plots. We further characterized the nature of these biskyrmions by their skyrmion densities. Evolution of the magnetic states with corresponding $\mathscr{T}$ and SSF as we cool down the system showed a crossover behavior at $T = 1.1$ and a transition to the biskyrmion ground state at $T = 0.55$. At $T = 1.1$, we observed a crossover from a paramagnetic state with finite chirality to a magnetic state with a diffused circular ring pattern without any prominent peaks, which can be seen as chiral filaments starting to form biskyrmions or thermal fluctuations of biskyrmion states. Below $T = 0.55$, the stabilization of the biskyrmion states was realized, which was reflected in hexagonal symmetrical peaks in SSF. The number and the size of the biskyrmions were shown to depend on the strength of the chiral spin interaction parameter.

ACKNOWLEDGMENTS

We acknowledge financial support from the Ministry of Education, Singapore, through Grant No. RG 138/22 and the use of the computational resources at the High Performance Computing Centre (HPCC) at NTU, Singapore, and the National Supercomputing Centre (NSCC), Singapore.

[1] A. Fert, N. Reyren, and V. Cros, Magnetic skyrmions: Advances in physics and potential applications, Nat. Rev. Mater. **2**, 17031 (2017).
[2] A. Fert, V. Cros, and J. Sampaio, Skyrmions on the track, Nat. Nanotechnol. **8**, 152 (2013).
[3] N. Nagaosa and Y. Tokura, Topological properties and dynamics of magnetic skyrmions, Nat. Nanotechnol. **8**, 899 (2013).
[4] A. N. Bogdanov and C. Panagopoulos, The emergence of magnetic skyrmions, Phys. Today **73**, 44 (2020).
[5] B. Göbel, A. Mook, J. Henk, and I. Mertig, Overcoming the speed limit in skyrmion racetrack devices by suppressing the skyrmion Hall effect, Phys. Rev. B **99**, 020405(R) (2019).
[6] K. Karube, J. S. White, D. Morikawa, C. D. Dewhurst, R. Cubitt, A. Kikkawa, X. Yu, Y. Tokunaga, T.-h. Arima, H. M. Rønnow, Y. Tokura, and Y. Taguchi, Disordered skyrmion phase stabilized by magnetic frustration in a chiral magnet, Sci. Adv. **4**, eaar7043 (2018).
[7] B. Dupé, M. Hoffmann, C. Paillard, and S. Heinze, Tailoring magnetic skyrmions in ultra-thin transition metal films, Nat. Commun. **5**, 4030 (2014).
[8] S. D. Pollard, J. A. Garlow, J. Yu, Z. Wang, Y. Zhu, and H. Yang, Observation of stable Néel skyrmions in cobalt/palladium multilayers with Lorentz transmission electron microscopy, Nat. Commun. **8**, 14761 (2017).
[9] A. Soumyanarayanan, M. Raju, A. L. Gonzalez Oyarce, A. K. C. Tan, M.-Y. Im, A. Petrović, P. Ho, K. H. Khoo, M. Tran, C. K. Gan, F. Ernult, and C. Panagopoulos, Tunable room-temperature magnetic skyrmions in Ir/Fe/Co/Pt multilayers, Nat. Mater. **16**, 898 (2017).
[10] N. Romming, C. Hanneken, M. Menzel, J. E. Bickel, B. Wolter, K. von Bergmann, A. Kubetzka, and R. Wiesendanger, Writing and deleting single magnetic skyrmions. Science **341**, 636 (2013).
[11] X. Z. Yu, N. Kanazawa, W. Z. Zhang, T. Nagai, T. Hara, K. Kimoto, Y. Matsui, Y. Onose, and Y. Tokura, Skyrmion flow

near room temperature in an ultralow current density. Nat. Commun. **3**, 988 (2012).

[12] X. Z. Yu, N. Kanazawa, Y. Onose, K. Kimoto, W. Z. Zhang, S. Ishiwata, Y. Matsui, and Y. Tokura, Near room-temperature formation of a skyrmion crystal in thin-films of the helimagnet FeGe, Nat. Mater. **10**, 106 (2011).

[13] X. Zhao, C. Jin, C. Wang, H. Du, J. Zang, M. Tian, R. Che, and Y. Zhang, Direct imaging of magnetic field-driven transitions of skyrmion cluster states in FeGe nanodisks, Proc. Natl. Acad. Sci. USA **113**, 4918 (2016).

[14] S. Kunitski, M. Perini, S. von Malottki, A. Kubetzka, R. Wiesendanger, K. von Bergmann, and S. Heinze, Isolated zero field sub-10 nm skyrmions in ultrathin Co films, Nat. Commun. **10**, 1 (2019).

[15] A. Tonomura, X. Yu, K. Yanagisawa, T. Matsuda, Y. Onose, N. Kanazawa, H. S. Park, and Y. Tokura, Real-space observation of skyrmion lattice in helimagnet MnSi thin samples, Nano Lett. **12**, 1673 (2012).

[16] M. Hirschberger, T. Nakajima, S. Gao, L. Peng, A. Kikkawa, T. Kurumaji, M. Kriener, Y. Yamasaki, H. Sagayama, H. Nakao *et al.*, Skyrmion phase and competing magnetic orders on a breathing kagomé lattice, Nat. Commun. **10**, 5831 (2019).

[17] C. Jin, Z.-A. Li, A. Kovács, J. Caron, F. Zheng, F. N. Rybakov, N. S. Kiselev, H. Du, S. Blügel, M. Tian *et al.*, Control of morphology and formation of highly geometrically confined magnetic skyrmions, Nat. Commun. **8**, 15569 (2017).

[18] S. Mühlbauer, B. Binz, F. Jonietz, C. Pfleiderer, A. Rosch, A. Neubauer, R. Georgii, and P. Böni, Skyrmion lattice in a chiral magnet, Science **323**, 915 (2009).

[19] X. Z. Yu, W. Koshibae, Y. Tokunaga, K. Shibata, Y. Taguchi, N. Nagaosa, and Y. Tokura, Transformation between meron and skyrmion topological spin textures in a chiral magnet, Nature (London) **564**, 95 (2018).

[20] X. Z. Yu, Y. Onose, N. Kanazawa, J. H. Park, J. H. Han, Y. Matsui, N. Nagaosa, and Y. Tokura, Real-space observation of a two-dimensional skyrmion crystal, Nature (London) **465**, 901 (2010).

[21] M. Hoffmann, B. Zimmermann, G. P. Müller, D. Schürhoff, N. S. Kiselev, C. Melcher, and S. Blügel, Antiskyrmions stabilized at interfaces by anisotropic Dzyaloshinskii-Moriya interactions, Nat. Commun. **8**, 308 (2017).

[22] A. K. Nayak, V. Kumar, T. Ma, P. Werner, E. Pippel, R. Sahoo, F. Damay, U. K. Rößler, C. Felser, and S. S. P. Parkin, Magnetic antiskyrmions above room temperature in tetragonal Heusler materials, Nature (London) **548**, 561 (2017).

[23] K. Niitsu, Y. Liu, A. C. Booth, X. Yu, N. Mathur, M. J. Stolt, D. Shindo, S. Jin, J. Zang, N. Nagaosa *et al.*, Geometrically stabilized skyrmionic vortex in FeGe tetrahedral nanoparticles, Nat. Mater. **21**, 305 (2022).

[24] T. Okubo, S. Chung, and H. Kawamura, Multiple-q states and the skyrmion lattice of the triangular-lattice heisenberg antiferromagnet under magnetic fields, Phys. Rev. Lett. **108**, 017206 (2012).

[25] C. D. Batista, S.-Z. Lin, S. Hayami, and Y. Kamiya, Frustration and chiral orderings in correlated electron systems, Rep. Prog. Phys. **79**, 084504 (2016).

[26] S.-Z. Lin and S. Hayami, Ginzburg-Landau theory for skyrmions in inversion-symmetric magnets with competing interactions, Phys. Rev. B **93**, 064430 (2016).

[27] A. O. Leonov and M. Mostovoy, Multiply periodic states and isolated skyrmions in an anisotropic frustrated magnet, Nat. Commun. **6**, 8275 (2015).

[28] Z. Wang, Y. Su, S.-Z. Lin, and C. D. Batista, Meron, skyrmion, and vortex crystals in centrosymmetric tetragonal magnets, Phys. Rev. B **103**, 104408 (2021).

[29] A. Farrell and T. Pereg-Barnea, Strong coupling expansion of the extended Hubbard model with spin-orbit coupling, Phys. Rev. B **89**, 035112 (2014).

[30] J. Chen, D.-W. Zhang, and J.-M. Liu, Exotic skyrmion crystals in chiral magnets with compass anisotropy, Sci. Rep. **6**, 29126 (2016).

[31] U. K. Roessler, A. Bogdanov, and C. Pfleiderer, Spontaneous skyrmion ground states in magnetic metals, Nature (London) **442**, 797 (2006).

[32] N. Mohanta, E. Dagotto, and S. Okamoto, Topological Hall effect and emergent skyrmion crystal at manganite-iridate oxide interfaces, Phys. Rev. B **100**, 064429 (2019).

[33] U. K. Rößler, A. A. Leonov, and A. N. Bogdanov, Skyrmionic textures in chiral magnets, J. Phys.: Conf. Ser. **200**, 022029 (2010).

[34] J. Iwasaki, A. J. Beekman, and N. Nagaosa, Theory of magnon-skyrmion scattering in chiral magnets, Phys. Rev. B **89**, 064412 (2014).

[35] S. D. Yi, S. Onoda, N. Nagaosa, and J. H. Han, Skyrmions and anomalous Hall effect in a Dzyaloshinskii-Moriya spiral magnet, Phys. Rev. B **80**, 054416 (2009).

[36] S. Hayami and Y. Motome, Néel- and Bloch-type magnetic vortices in Rashba metals, Phys. Rev. Lett. **121**, 137202 (2018).

[37] S. Hayami and Y. Motome, Effect of magnetic anisotropy on skyrmions with a high topological number in itinerant magnets, Phys. Rev. B **99**, 094420 (2019).

[38] A. V. Bezvershenko, A. K. Kolezhuk, and B. A. Ivanov, Stabilization of magnetic skyrmions by RKKY interactions, Phys. Rev. B **97**, 054408 (2018).

[39] S. Hayami and R. Yambe, Field-direction sensitive skyrmion crystals in cubic chiral systems: Implication to 4f-electron compound EuPtSi, J. Phys. Soc. Jpn. **90**, 073705 (2021).

[40] D. S. Kathyat, A. Mukherjee, and S. Kumar, Microscopic magnetic Hamiltonian for exotic spin textures in metals, Phys. Rev. B **102**, 075106 (2020).

[41] D. S. Kathyat, A. Mukherjee, and S. Kumar, Electronic mechanism for nanoscale skyrmions and topological metals, Phys. Rev. B **103**, 035111 (2021).

[42] D. S. Kathyat, A. Mukherjee, and S. Kumar, Antiskyrmions and Bloch skyrmions in magnetic Dresselhaus metals, Phys. Rev. B **104**, 184434 (2021).

[43] A. Mukherjee, D. S. Kathyat, and S. Kumar, Engineering antiferromagnetic skyrmions and antiskyrmions at metallic interfaces, Phys. Rev. B **105**, 075102 (2022).

[44] S. Gao, H. D. Rosales, F. A. Gómez Albarracín, V. Tsurkan, G. Kaur, T. Fennell, P. Steffens, M. Boehm, P. Čermák, A. Schneidewind, E. Ressouche, D. C. Cabra, C. Rüegg, and O. Zaharko, Fractional antiferromagnetic skyrmion lattice induced by anisotropic couplings, Nature (London) **586**, 37 (2020).

[45] H. D. Rosales, D. C. Cabra, and P. Pujol, Three-sublattice skyrmion crystal in the antiferromagnetic triangular lattice, Phys. Rev. B **92**, 214439 (2015).

[46] A. Mukherjee, D. S. Kathyat, and S. Kumar, Antiferromagnetic skyrmions and skyrmion density wave in a Rashba-coupled Hund insulator, Phys. Rev. B **103**, 134424 (2021).

[47] A. A. Kovalev and S. Sandhoefner, Skyrmions and anti-skyrmions in quasi-two-dimensional magnets, Front. Phys. **6**, 403451 (2018).

[48] R. Ozawa, S. Hayami, and Y. Motome, Zero-field skyrmions with a high topological number in itinerant magnets, Phys. Rev. Lett. **118**, 147205 (2017).

[49] X. Z. Yu, Y. Tokunaga, Y. Kaneko, W. Z. Zhang, K. Kimoto, Y. Matsui, Y. Taguchi, and Y. Tokura, Biskyrmion states and their current-driven motion in a layered manganite, Nat. Commun. **5**, 1 (2014).

[50] L. Peng, Y. Zhang, W. Wang, M. He, L. Li, B. Ding, J. Li, Y. Sun, X.-G. Zhang, J. Cai, S. Wang, G. Wu, and B. Shen, Real-space observation of nonvolatile zero-field biskyrmion lattice generation in MnNiGa magnet, Nano Lett. **17**, 7075 (2017).

[51] S. Zuo, K. Qiao, Y. Zhang, T. Zhao, C. Jiang, and B. Shen, Spontaneous biskyrmion lattice in a centrosymmetric rhombohedral rare-earth magnet with easy-plane anisotropy, Nano Lett. **23**, 550 (2023).

[52] J. C. Loudon, A. C. Twitchett-Harrison, D. Cortés-Ortuño, M. T. Birch, L. A. Turnbull, A. Štefančič, F. Y. Ogrin, E. O. Burgos-Parra, N. Bukin, A. Laurenson, H. Popescu, M. Beg, O. Hovorka, H. Fangohr, P. A. Midgley, G. Balakrishnan, and P. D. Hatton, Do images of biskyrmions show type-II bubbles? Adv. Mater. **31**, 1806598 (2019).

[53] Y. Yao, B. Ding, J. Cui, X. Shen, Y. Wang, W. Wang, and R. Yu, Magnetic hard nanobubble: A possible magnetization structure behind the bi-skyrmion, Appl. Phys. Lett. **114**, 102404 (2019).

[54] B. Göbel, J. Henk, and I. Mertig, Forming individual magnetic biskyrmions by merging two skyrmions in a centrosymmetric nanodisk, Sci. Rep. **9**, 9521 (2019).

[55] D. Capic, D. A. Garanin, and E. M. Chudnovsky, Stabilty of biskyrmions in centrosymmetric magnetic films, Phys. Rev. B **100**, 014432 (2019).

[56] D. Capic, D. A. Garanin, and E. M. Chudnovsky, Biskyrmion lattices in centrosymmetric magnetic films, Phys. Rev. Res. **1**, 033011 (2019).

[57] R. Eto, R. Pohle, and M. Mochizuki, Low-energy excitations of skyrmion crystals in a centrosymmetric Kondo-lattice magnet: Decoupled spin-charge excitations and nonreciprocity, Phys. Rev. Lett. **129**, 017201 (2022).

[58] C.-J. Wang, P. Wang, Y. Zhou, W. Wang, F. Shi, and J. Du, Formation of magnetic biskyrmions mediated by an intrinsic emergent monopole-antimonopole pair, npj Quantum Mater. **7**, 78 (2022).

[59] W.-J. Hu, S.-S. Gong, and D. N. Sheng, Variational Monte Carlo study of chiral spin liquid in quantum antiferromagnet on the triangular lattice, Phys. Rev. B **94**, 075131 (2016).

[60] D. Sen and R. Chitra, Large-U limit of a Hubbard model in a magnetic field: Chiral spin interactions and paramagnetism, Phys. Rev. B **51**, 1922 (1995).

[61] B. Bauer, L. Cincio, B. P. Keller, M. Dolfi, G. Vidal, S. Trebst, and A. W. Ludwig, Chiral spin liquid and emergent anyons in a Kagome lattice Mott insulator, Nat. Commun. **5**, 5137 (2014).

[62] R. Samajdar, M. S. Scheurer, S. Chatterjee, H. Guo, C. Xu, and S. Sachdev, Enhanced thermal Hall effect in the square-lattice Néel state, Nat. Phys. **15**, 1290 (2019).

[63] A. Wietek, A. Sterdyniak, and A. M. Läuchli, Nature of chiral spin liquids on the kagome lattice, Phys. Rev. B **92**, 125122 (2015).